


RESEARCH

Open Access



Conditional knockout of *Tsc1* in RORyt-expressing cells induces brain damage and early death in mice

Yafei Deng^{1†}, Qinglan Yang^{1†}, Yao Yang², Yana Li¹, Hongyan Peng¹, Shuting Wu¹, Shuju Zhang¹, Baige Yao³, Shuhui Li⁴, Yuan Gao⁵, Xiaohui Li^{2*}, Liping Li^{1*} and Youcai Deng^{2*} 

Abstract

Background: Tuberous sclerosis complex 1 (*Tsc1*) is known to regulate the development and function of various cell types, and RORyt is a critical transcription factor in the immune system. However, whether *Tsc1* participates in regulating RORyt-expressing cells remains unknown.

Methods: We generated a mouse model in which *Tsc1* was conditionally deleted from RORyt-expressing cells (*Tsc1*^{RORyt}) to study the role of RORyt-expressing cells with *Tsc1* deficiency in brain homeostasis.

Results: Type 3 innate lymphoid cells (ILC3s) in *Tsc1*^{RORyt} mice displayed normal development and function, and the mice showed normal Th17 cell differentiation. However, *Tsc1*^{RORyt} mice exhibited spontaneous tonic-clonic seizures and died between 4 and 6 weeks after birth. At the age of 4 weeks, mice in which *Tsc1* was specifically knocked out in RORyt-expressing cells had cortical neuron defects and hippocampal structural abnormalities. Notably, over-activation of neurons and astrogliosis were observed in the cortex and hippocampus of *Tsc1*^{RORyt} mice. Moreover, expression of the γ -amino butyric acid (GABA) receptor in the brains of *Tsc1*^{RORyt} mice was decreased, and GABA supplementation prolonged the lifespan of the mice to some extent. Further experiments revealed the presence of a group of rare RORyt-expressing cells with high metabolic activity in the mouse brain.

Conclusions: Our study verifies the critical role of previously unnoticed RORyt-expressing cells in the brain and demonstrates that the *Tsc1* signaling pathway in RORyt-expressing cells is important for maintaining brain homeostasis.

Keywords: RORyt-expressing cells, *Tsc1*, GABA, Seizure

* Correspondence: lpsh008@aliyun.com; 13974871993@163.com; youcai.deng@tmmu.edu.cn

[†]Yafei Deng and Qinglan Yang contributed equally to this work.

²Institute of Materia Medica, College of Pharmacy, Army Medical University (Third Military Medical University), Chongqing 400038, China

¹Hunan Children's Research Institute (HCRI), Hunan Children's Hospital, Changsha 410000, China

Full list of author information is available at the end of the article



© The Author(s). 2021 **Open Access** This article is licensed under a Creative Commons Attribution 4.0 International License, which permits use, sharing, adaptation, distribution and reproduction in any medium or format, as long as you give appropriate credit to the original author(s) and the source, provide a link to the Creative Commons licence, and indicate if changes were made. The images or other third party material in this article are included in the article's Creative Commons licence, unless indicated otherwise in a credit line to the material. If material is not included in the article's Creative Commons licence and your intended use is not permitted by statutory regulation or exceeds the permitted use, you will need to obtain permission directly from the copyright holder. To view a copy of this licence, visit <http://creativecommons.org/licenses/by/4.0/>. The Creative Commons Public Domain Dedication waiver (<http://creativecommons.org/publicdomain/zero/1.0/>) applies to the data made available in this article, unless otherwise stated in a credit line to the data.

Introduction

Tuberous sclerosis complex 1 (*Tsc1*), which forms a heterodimeric complex with tuberous sclerosis complex 2 (*Tsc2*), controls and mediates major processes, including protein and lipid synthesis, autophagy, and cell survival and proliferation [1]. Disruption of the *Tsc1-Tsc2* complex results in various human diseases, such as hamartomas in multiple organs, cortical dysplasia, hypomelanotic macules, and cancers [2, 3]. Previous studies found that targeted homozygous *Tsc1* or *Tsc2* mutations lead to death during the mid-embryonic period [4]. Mice with conditional *Tsc1* knockout in neurons or astrocytes exhibit abnormal brain structure and function [5]. For example, mice with neuronal *Tsc1* loss develop spontaneous seizures, macroencephaly, and hydrocephalus [6, 7]. Astrocyte-specific *Tsc1*-knockout mice also display epilepsy and some alterations in brain structure [8]. *Tsc1* also plays a critical role in regulating the development and functions of immune cells, such as T cells and NK cells. Deletion of *Tsc1* in CD4⁺ cells resulted in increased Th1 and Th17 cells differentiation [9], while conditional *Tsc1* deletion in Tregs impaired their suppressive activity [10]. Hematopoietic-specific deletion of *Tsc1* resulted in an activated and pro-apoptotic phenotype in NK cells [11]. However, the physiological role of *Tsc1*, especially in innate lymphoid cells (ILCs), remains largely unknown.

According to previous studies, ROR γ t is a critical transcription factor for type 3 innate lymphoid cells (ILC3s) and Th17 cells [12, 13]. ROR γ t deficiency leads to the failure of lymphoid tissue inducer cells (LTi cells) and failure to generate ILC3 subsets [14, 15]. Therefore, ROR γ t-Cre mice are now commonly used as an animal model to study the roles of specific genes in regulating ILC3s or Th17 cells. However, whether *Tsc1* participates in regulating ROR γ t-expressing cells remains unknown.

In this study, we found that mice with conditional *Tsc1* deletion from ROR γ t-expressing cells (*Tsc1*^{ROR γ t} mice) had numbers of ILC3s in the intestinal lamina propria layer and Th17 cells in the spleen comparable to those of their control littermates. However, *Tsc1*^{ROR γ t} mice died in a narrow timeframe between 4 and 6 weeks after birth. As previous studies showed that *Tsc1* deletion in neurons or astrocytes led to brain damage and death [6–8]; here, we further reveal that *Tsc1*^{ROR γ t} mice show obvious brain damage, including cortical neuron defects, hippocampal structural abnormalities, neuron over-activation, and astrogliosis in the cortex and hippocampus. Mechanistically, the loss of *Tsc1* in ROR γ t-expressing cells resulted in lower γ -amino butyric acid (GABA) receptor expression in the brain, and GABA supplementation prolonged the lifespan of *Tsc1*^{ROR γ t} mice to some extent.

Methods

Animals

C57BL/6 *Rorc*-Cre (B6.FVB-Tg (*Rorc*-cre)1Litt/J, stock No. 022791) mice [16] and *Tsc1*^{fl/fl} (*Tsc1*^{tm1Djk/J}), stock No. 005680) mice [17] were obtained from The Jackson Laboratory (Sacramento, CA, USA). All mice were bred under specific pathogen-free conditions at the Experimental Animal Center of Hunan Children's Hospital (Changsha, China). For the GABA supplementation experiment, the *Tsc1*^{ROR γ t} mice and control littermates were fed GABA through the drinking water (0.5 mg/ml) at 3 weeks after weaning.

Preparation of single-cell suspensions

Single-cell suspensions were prepared as previously described [18, 19]. Briefly, mice were anesthetized with an isoflurane vaporizer (4–5% v/v). Spleen tissues were ground and passed through a 70- μ m stainless steel mesh, and pellets were collected after centrifugation (450 \times g, room temperature, 10 min). Spleen mononuclear cells were separated from the pellets by lysing erythrocytes. The small intestines were opened longitudinally and washed with PBS (pH 7.4, Sigma-Aldrich, St. Louis, MO, USA) to remove the contents after Peyer's patches had been removed. Then, the intestines were cut into segments 4–5 cm in length and gently shaken in D-Hanks' solution (pH 7.4) containing 10 mM HEPES, 5 mM EDTA, 1 mM DTT, and 10% fetal bovine serum (FBS) for 20 min at 37 °C. The remaining intestinal tissues were rinsed with Hanks' solution and then digested with 1 mg/ml collagenase II (Gibco, Waltham, MA, USA) in Hanks' solution (pH 7.4) supplemented with 10% FBS for 40 min at 37 °C with gentle shaking. The collected digests were filtered through a 100- μ m mesh and enriched by centrifugation (450 \times g, room temperature, and 10 min) with a 25% Percoll solution (GE Healthcare, Pittsburgh, PA, USA) in RPMI 1640 medium (Gibco).

Antibodies and flow cytometry

All antibodies used for staining and subsequent flow cytometry analysis are listed in Supplemental Table 1. We confirmed the species reactivity for all antibodies according to the manufacturer's directions and performed preliminary experiments to determine the appropriate dilutions for all antibodies. Standard protocols were used for flow cytometry [19, 20]. Briefly, single-cell suspensions were obtained from the spleen and intestinal lamina propria tissues of the mice. To analyze surface markers, 2 \times 10⁶ cells were incubated with staining buffer (PBS containing 2% mouse serum, 2% horse serum, and anti-CD16/CD32 blocking antibodies (BioLegend, San Diego, CA, USA)) and the indicated surface antibodies for 15 min at room temperature.

To detect IL-17A and IL-22, 2×10^6 cells were stimulated with IL-23 (BioLegend) or PMA/ionomycin (BD Biosciences, San Diego, CA, USA) for 4 h in the presence of BD Golgi Plug™ protein transport inhibitor (BD Biosciences) at 37 °C. Then, the cells were fixed with a Fixation/Permeabilization Solution Kit (BD Biosciences) according to the manufacturer's instructions.

For RORγt staining, cells were stained with antibodies against surface markers, permeabilized with the Foxp3/Transcription Factor Staining Buffer Set Kit (eBioscience, San Diego, CA, USA), and then stained with anti-RORγt antibody. Lineage (Lin) markers included CD3e, CD19, B220 and Gr-1. All of the isotype-matched control antibodies were purchased from BioLegend and BD and used at the same concentration as the test antibodies. All flow cytometry experiments were performed with a BD FACS Canto™ or BD FACS LSRFortessa™ instrument (BD Biosciences). Data were analyzed with FlowJo software (version 10.0, FlowJo LLC, Ashland, OR, USA). The lines indicate median values for each group.

Histological analysis

The mice were anaesthetized with an isoflurane vaporizer (4–5% v/v), and all tissues were collected as described in our previous reports [18, 21]. Histological structures of the heart, lung, kidney, spleen, stomach, liver, and brain were analyzed by standard hematoxylin-eosin (HE) staining and assessed for the presence of pathomorphological changes by trained pathologists who were blinded to the experimental groups. The Nissl bodies in the brain were detected by Nissl staining. Briefly, the tissues were fixed in 10% neutral buffered formalin for at least 24 h, embedded in paraffin, and cut into 4-μm-thick sections. The paraffin sections were stained with HE or Nissl staining solutions after they had been processed according to standard protocols [22].

All antibodies used for immunofluorescence staining are listed in Supplemental Table 1. The brain sections were incubated with a polyclonal rat anti-mouse glial fibrillary acidic protein (GFAP) antibody (eBioscience) and/or polyclonal rabbit anti-mouse neuronal nuclei antigen (NeuN) antibody (eBioscience) in 10% goat serum overnight at 4 °C after deparaffinization, rehydration, and antigen retrieval. The sections were washed with 1× PBST (1× PBS, 0.05% Tween-20), incubated with secondary antibodies (Alexa Fluor® 488-conjugated goat anti-rat IgG (H+L) for GFAP and Alexa Fluor® 594-conjugated goat anti-rabbit IgG (H+L) for NeuN) for 1 h at room temperature and then stained with DAPI. Coverslips containing samples from all organs, except for the brain, subjected to HE staining were scanned using an Olympus VS200 slide scanner (Olympus, Japan) and visualized with OlyVIA version 3.2 software (Olympus). Coverslips containing brain samples were scanned using

Pannoramic DESK (3D HISTECH, Budapest, Hungary) and visualized with CaseViewer software (3D HISTECH). Measurements of cortical thickness and cell scattering width in the CA1, CA3, and dentate gyrus (DG) regions of the hippocampus were performed using CaseViewer software (3D HISTECH). Quantitative analyses of the area fraction of GFAP⁺ astrocytes, NeuN⁺ neurons, and Nissl bodies were performed using ImageJ software version 1.52v (National Institutes of Health, Bethesda, MD, USA) [23]. The investigators who acquired and analyzed the images were blinded to the experimental groups.

Electrocardiogram measurement

The mice were anaesthetized with an isoflurane vaporizer (4–5% v/v), and the electrocardiogram (ECG) was measured and recorded by electrocardiography (Mindray, Shenzhen, China) according to the operation manual.

Detection of mRNA levels by real-time RT-PCR

Briefly, mice were anesthetized with an isoflurane vaporizer (4–5% v/v), and whole-brain parenchyma and thymus tissues then were harvested. Total RNA was extracted and reverse transcribed into cDNA using standard protocols as previously described [24]. Total RNA was extracted from the brain and thymus tissues using TRIzol reagent (Invitrogen, Waltham, MA, USA), and cDNA was synthesized using a First Stand cDNA Synthesis Kit (DBI Bioscience, Ludwigshafen, Germany). Real-time PCR was performed using Bestar® SYBR Green qPCR Master Mix (DBI Bioscience, San Diego, CA, USA). The cycle threshold (Ct) values were normalized to the internal control (*gapdh*). The primer sequences for qRT-PCR were obtained from the Primer Bank, and the primer pairs used in the present study are shown in Supplemental Table 2.

Western blotting

Briefly, mice were anesthetized with an isoflurane vaporizer (4–5% v/v). Then, whole-brain parenchyma and thymus tissues were harvested and lysed with RIPA buffer (Sigma-Aldrich), separated by SDS-PAGE, transferred to PVDF membranes (GE Healthcare, Pittsburgh, PA, USA), and incubated with anti-RORγt antibody in 5% BSA [23]. Immunoblotting was performed using HRP-conjugated secondary antibodies for visualization.

Seizure test

Seizures were induced with pentylenetetrazole (PTZ) as previously described [25]. PTZ (50 mg/kg, Sigma-Aldrich) was administered intraperitoneally at 10-min intervals to post-natal days (PNDs) 28 mice. The injections were administered until the mice died (1–3 injections). Seizure latency was recorded as the time from PTZ injection to

seizure occurrence. Observers were blinded to the genotypes of the mice.

Single-cell data analysis

The raw gene count expression matrix and metadata from embryonic day 14.5 mouse cerebral cortex scRNA-seq datasets were downloaded from GEO (<https://www.ncbi.nlm.nih.gov/geo/>) (accession ID: GSE123335) [26] for analysis. Dimensional reduction, clustering, and analysis of scRNA-seq data were performed with the R package Seurat version 3 [27]. Cells with a RORC gene expression level ≥ 1 were considered RORyt-positive cells. The top 25% of the median of all expressed genes in RORyt-positive cells were considered highly expressed genes and used for KEGG enrichment analysis based on ClueGO to analyze the potential functions of RORyt-positive cells [28]. Gene set variation analysis (GSVA), a nonparametric and unsupervised software algorithm, was used to assess KEGG pathway activation with the R package GSVA [29].

Statistical analyses

All quantitative data were transferred to Excel, and statistical analyses were carried out with SPSS software for Windows (version 21, SPSS Inc., Chicago, Illinois, USA). Data are presented as the means \pm SEMs. For comparisons between two independent experimental groups, an unpaired two-tailed Student's *t* test was used when data were normally distributed. When more than two independent groups were compared, one-way ANOVA followed by Tukey's test was performed. The Wilcoxon

test was used to compare the difference in KEGG pathway scores estimated by GSVA between RORyt-positive and RORyt-negative cells with R (version 3.5.1) [30]. A *p* value less than 0.05 was considered to indicate statistical significance. Each analysis included $n = 4$ –18 replicates per group, and the results are representative of at least two independent experiments. The sample size for each experiment is indicated in the corresponding figure legend. All graphs were produced using GraphPad Prism 5.0 for Windows (GraphPad Software Inc., La Jolla, CA, USA).

Results

Deletion of *Tsc1* in RORyt-expressing cells resulted in the unexpected death of mice

To investigate whether *Tsc1* deletion would affect RORyt-expressing cells, we crossed *Tsc1* floxed (*Tsc1*^{fl/fl}) mice with RORyt-Cre mice to obtain *Tsc1*^{fl/fl}-RORyt^{Cre+} mutant mice in which *Tsc1* was deleted from only RORyt-expressing cells (referred to as *Tsc1*^{RORyt} mice), while *Tsc1*^{fl/fl}-RORyt^{Cre-} littermates were used as control mice. We initially aimed to explore the effects of *Tsc1* deficiency on ILC3s and Th17 cells; however, all *Tsc1*^{RORyt} mice unexpectedly died between PNDs 30 and PNDs 40, with a median survival time of 33 days (Fig. 1a, b). However, mice with heterozygous *Tsc1* knockout in RORyt-expressing cells (*Tsc1*^{fl/-}-RORyt^{Cre}) had a lifespan similar to that of control littermates (Fig. 1a). The *Tsc1*^{RORyt} mice had a normal weight and did not display gross morphological abnormalities upon comparison with control littermates before their death (Fig. 1c, d).

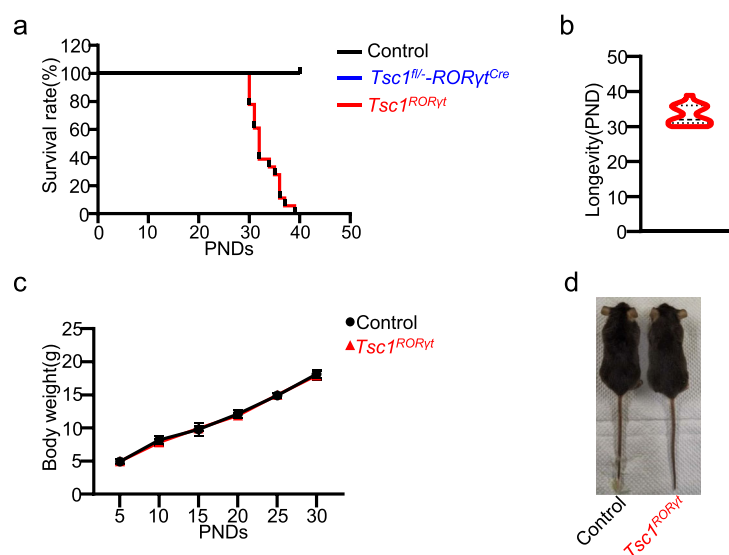


Fig. 1 The deletion of *Tsc1* in RORyt-expressing cells resulted in the unexpected death of mice. **a–d** The survival rate (**a**), longevity (**b**), body weight (**c**), and appearance (**d**) of *Tsc1*^{RORyt} mice and control littermates. One-way ANOVA (**a**). $n = 9$ –18 (**a**), $n = 18$ (**b**), $n = 6$ (**c**). Unpaired two-tailed Student's *t* test (**c**).

ILC3s and Th17 cells in *Tsc1*-deficient *RORγt*-expressing cells showed normal phenotypes

First, we postulated that the early death of the mice had been induced by the knockout of *Tsc1* in ILC3s or Th17 cells, as according to the description of mice homozygous for the *RORC* mutant allele (*RORγt*^{GFP/GFP}) from The Jackson Laboratory, *RORγt*-deficient mice were reported to die at the age of 9–32 weeks [16]. Because these *Tsc1*^{RORγt} mice died between PNDs 30 and PNDs 40, all analyses of the mice were conducted at PNDs 28 unless specified otherwise. Flow cytometry analysis showed that *Tsc1*^{RORγt} mice had numbers of ILC3s and ILC3 subsets comparable to those of their control littermates (Fig. 2a, b). Moreover, *Tsc1* deficiency in *RORγt*-expressing cells did not affect the expression of IL-17A or IL-22 (Fig. 2c, d), the main cytokines expressed in ILC3s, in this cell type [31]. As *RORγt* is also expressed in Th17 cells, we determined the ratio of Th17 cells in these mice and found that ratios of CD4⁺ T cells, CD8⁺

T cells, and Th17 cells in the intestinal lamina propria layer (LPL) and spleen were comparable in *Tsc1*^{RORγt} mice and their control littermates (Fig. 2e–h).

To further investigate the cause of death, we assessed pathological changes in several critical organs, including the heart, lung, kidney, spleen, stomach, and liver, of *Tsc1*^{RORγt} mice by hematoxylin-eosin (HE) staining. *Tsc1*^{RORγt} mice did not display significant pathomorphological changes that would have led to their death (Fig. 3a–f). Meanwhile, ECG measurements also revealed that *Tsc1*^{RORγt} mice had normal cardiac function (Fig. 3g). These results strongly suggest that the death of the mice caused by *Tsc1* deficiency in *RORγt*-expressing cells was independent of ILC3s and Th17 cells.

***Tsc1*^{RORγt} mice exhibit spontaneous tonic-clonic seizures with neuronal defects**

Unexpectedly, the *Tsc1*^{RORγt} mice often suffered megascopic spontaneous seizures characterized by generalized

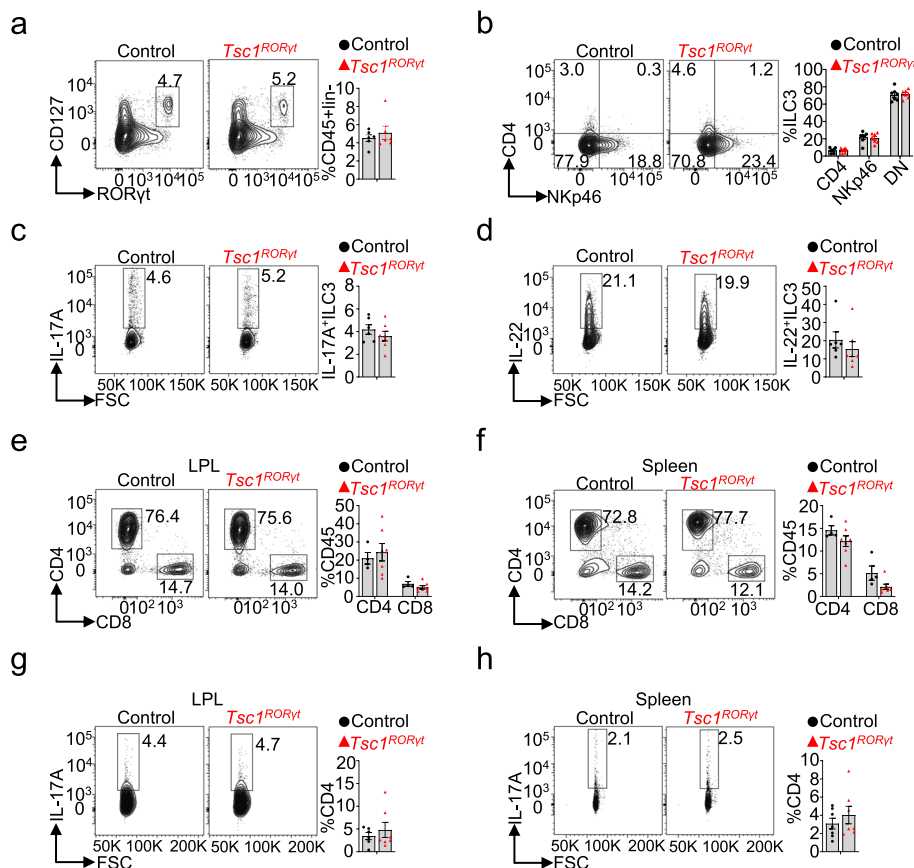


Fig. 2 ILC3s and Th17 cells from *Tsc1*-deficient *RORγt*-expressing cells showed normal phenotypes. **a, b** Flow cytometry analysis and cumulative frequencies of total ILC3s (**a**) and their subsets (**b**) in the LPL of *Tsc1*^{RORγt} mice. **c, d** Flow cytometry analysis and cumulative frequencies of IL-17-producing and IL-22-producing ILC3s in the small intestine LPL of *Tsc1*^{RORγt} mice. **e, f** Flow cytometry analysis and cumulative frequencies of CD4⁺ T cells and CD8⁺ T cells in the LPL (**e**) and spleen (**f**), respectively. **g, h** Flow cytometry analysis and cumulative frequencies of IL-17-producing CD4⁺ T cells in the LPL (**g**) and spleen (**h**), respectively. Each dot represents one mouse; error bars represent SEMs. Unpaired two-tailed Student's t test (**a–h**)

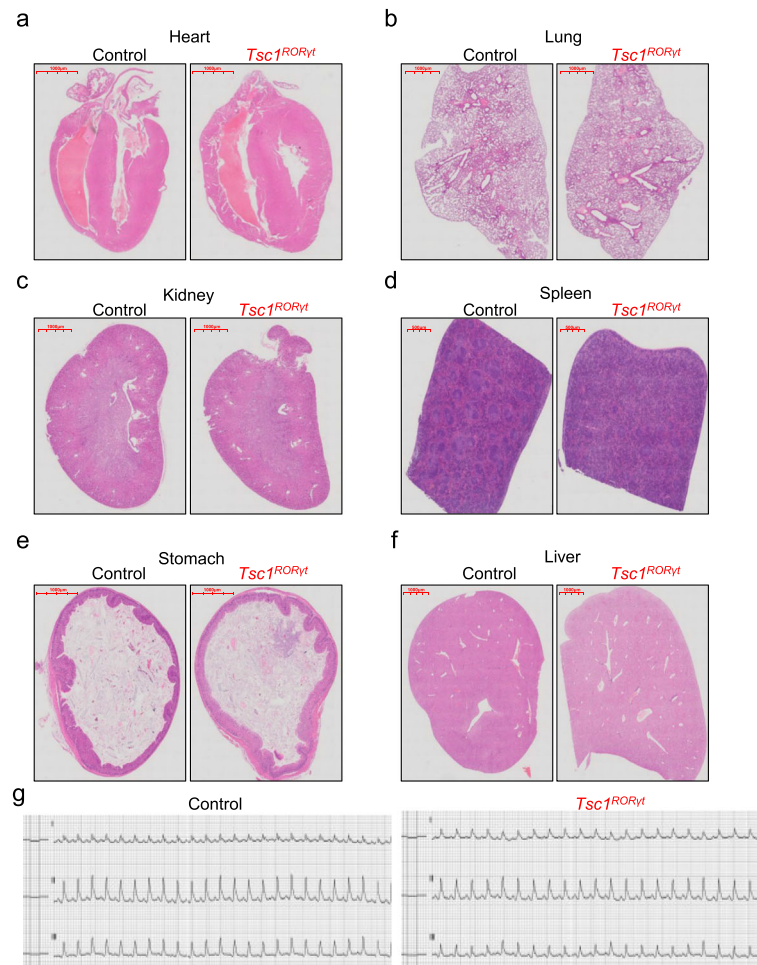


Fig. 3 *Tsc1*^{RORyt} mice did not display significant pathomorphological changes in various tissues and exhibited normal cardiac function. **a** HE staining and representative images of the heart, lung, kidney, spleen, stomach, and liver of *Tsc1*^{RORyt} mice and control littermates. **b** Representative ECG measurements from *Tsc1*^{RORyt} mice and control littermates. *n* = 5 animals per group. All HE staining images were captured from scans of whole-tissue slices. Scale bars: 500 μm (**d**) and 1000 μm (**a, b, c, e, f**)

tonic-clonic activity before PNDs 28 (Supplemental Video 1). The seizure activity became more severe with increasing age, ultimately resulting in wild jumping and death (Fig. 4a and Supplemental Video 2). We next assessed pathomorphological changes in the brain to further investigate the cause of death in the *Tsc1*^{RORyt} mice. The brain size and cerebral cortical thickness of the *Tsc1*^{RORyt} mice were the same as those of control littermates (Fig. 4b, c). However, neurons in the cerebral cortex of *Tsc1*^{RORyt} mice appeared swollen and necrotic, unlike those of control littermates (Fig. 4d). The hippocampus of *Tsc1*^{RORyt} mice also exhibited defects in organization. HE staining showed that structure of the dentate gyrus (DG) in the hippocampus was disorganized, and the arrangement of neurons was also disordered in the *Tsc1*^{RORyt} mice (Fig. 4e). Immunofluorescence staining for NeuN showed that the CA1 and CA3 pyramidal cell layers and DG granule cell layer were organized in an irregular fashion and that cells

in these regions were discrete in *Tsc1*^{RORyt} mice. Quantitative analysis revealed increased cell scattering widths in the CA1, CA3, and DG cell layers of *Tsc1*^{RORyt} mice (Fig. 4f). These results suggest that the loss of *Tsc1* in *RORyt*-expressing cells resulted in neuronal perturbations in the cortex and structural abnormalities in the hippocampus.

Abnormal activation of neurons and astrogliosis in the cortex and hippocampus of *Tsc1*^{RORyt} mice

Seizures are usually characterized by the abnormal and excessive synchronous firing of neurons [32]. Nissl bodies are usually regarded as an indicator of neuronal activation, in the brain [33]; therefore, we determined the number of Nissl bodies in CA1 and CA3 pyramidal cell layers and the DG granule cell layer of both control and *Tsc1*^{RORyt} mice. Compared with control littermates, *Tsc1*^{RORyt} mice exhibited an increased number of Nissl bodies with a complex microstructure, as evidenced by

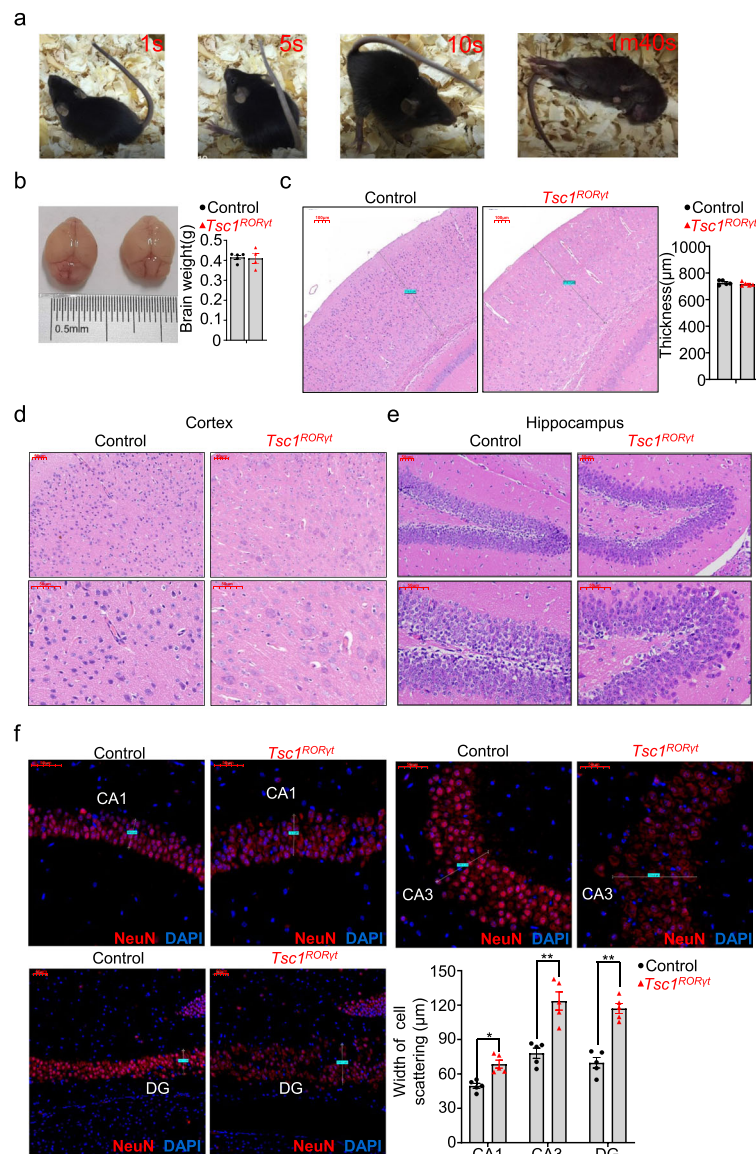


Fig. 4 *Tsc1^{RORyt}* mice exhibited spontaneous tonic-clonic seizures with neuronal defects. **a** Representative images of spontaneous generalized tonic-clonic seizures at different phases observed in the *Tsc1^{RORyt}* mice. These images were extracted from a video of *Tsc1^{RORyt}* mice housed with control littermates. **b** The brain weights of *Tsc1^{RORyt}* mice and control littermates. **c** Representative images of HE staining and thickness of the cortex of the brains of *Tsc1^{RORyt}* mice and control littermates. **d, e** Representative HE staining images of the cortex (**d**) and hippocampus (**e**) of *Tsc1^{RORyt}* mice and control littermates. **f** Representative images of NeuN immunostaining (red) and the cell scattering width in the CA and DG regions of the hippocampus from *Tsc1^{RORyt}* mice and control littermates. Each dot represents one mouse, and error bars represent SEMs; * $p < 0.05$, ** $p < 0.01$. Unpaired two-tailed Student's *t* test (**b, c, f**). All images were captured from scans of whole-brain slices. Magnification: $\times 10$ (**c**), $\times 20$ (upper panels in **d, e**), and $\times 40$ (lower panels in **d, e, f**). Scale bars: $50 \mu\text{m}$ (**d, e, f**) and $100 \mu\text{m}$ (**c**)

deeper staining and an increased area fraction of Nissl bodies in the cortex and hippocampus, indicating that *Tsc1^{RORyt}* mice exhibited abnormal neuronal activation (Supplemental Fig. 1a and Fig. 5a–e). However, the deletion of *Tsc1* in RORyt-expressing cells did not affect the number of total neurons in the CA1 or CA3 pyramidal cell layer or the DG granule cell layer, as indicated by quantitative analysis of the area fraction of NeuN⁺ neurons (Supplemental Fig. 1b and Fig. 5f–h).

Astroglialosis, which refers to an abnormal increase in astrocytes, usually occurs when an insult to the brain is sustained and often presents in patients with tuberous sclerosis syndrome or epilepsy [34]; elevated GFAP expression is a marker of astroglialosis [35]. We observed weakly stained astrocytes in the cerebral cortex of control mice; moreover, the area fraction of GFAP⁺ astrocytes was obviously increased in the cortex of *Tsc1^{RORyt}* mice compared to control littermates (Fig. 5f, h). Moreover, compared with that of control littermates,

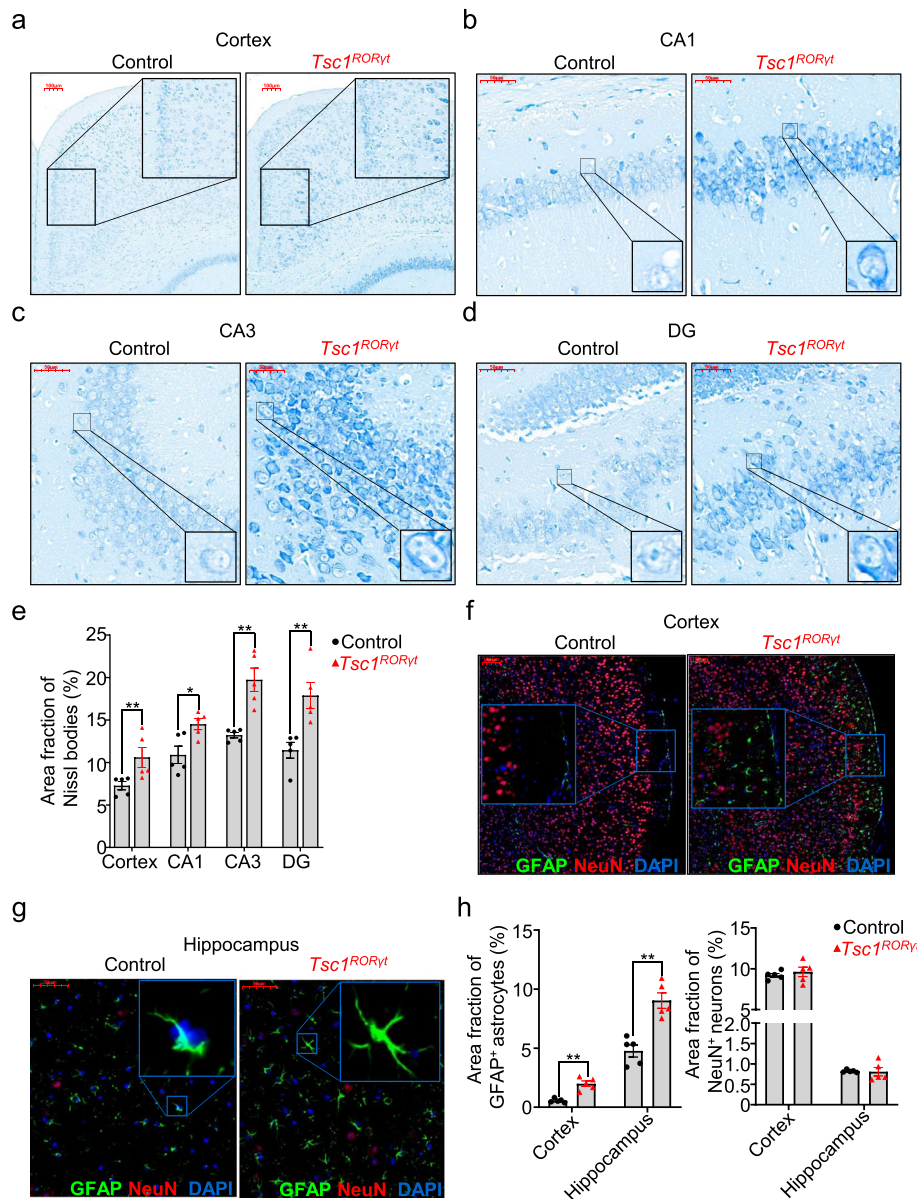


Fig. 5 Abnormal activation of neurons and astrogliosis in the cortex and hippocampus of *Tsc1*^{RORyt} mice. **a–d** Representative images of Nissl staining of the cerebral cortex (**a**) and different regions of the hippocampus (**b–d**) of *Tsc1*^{RORyt} mice and control littermates. **e** Statistical analysis of the area fraction of Nissl bodies shown in **a–d**. **f–h** Representative images of GFAP immunostaining (green) (**f** and **j**) and the area fraction of GFAP⁺ astrocytes and NeuN⁺ neurons (**h**) in the cerebral cortex (**f**) and hippocampus (**j**) of *Tsc1*^{RORyt} mice and control littermates. Each dot represents one mouse and the error bars represent SEMs; * $p < 0.05$ and ** $p < 0.01$. Unpaired two-tailed Student's *t* test (**e**, **g**). The locations of the magnified box are identified in the original image. All images were captured from scans of whole-brain slices. Magnification: 10 \times (**a**, **f**) and $\times 40$ (**b**, **c**, **d**, **g**). Scale bars: 50 μ m (**b**, **c**, **d**, **g**) and 100 μ m (**a**, **f**)

increased GFAP expression was also found throughout the hippocampus of *Tsc1*^{RORyt} mice, in which GFAP⁺ astrocytes were widely distributed, especially in the DG region (Supplemental Fig. 1b and Fig. 5g, h).

Thus, deletion of *Tsc1* from RORyt-expressing cells did not affect the ratios or phenotypes of ILC3s or Th17 cells but resulted in abnormal activation of neurons and

astrogliosis, which might have been responsible for the seizures observed in the *Tsc1*^{RORyt} mice.

Defects in the GABA signaling pathway are at least partially responsible for seizures and death in *Tsc1*^{RORyt} mice

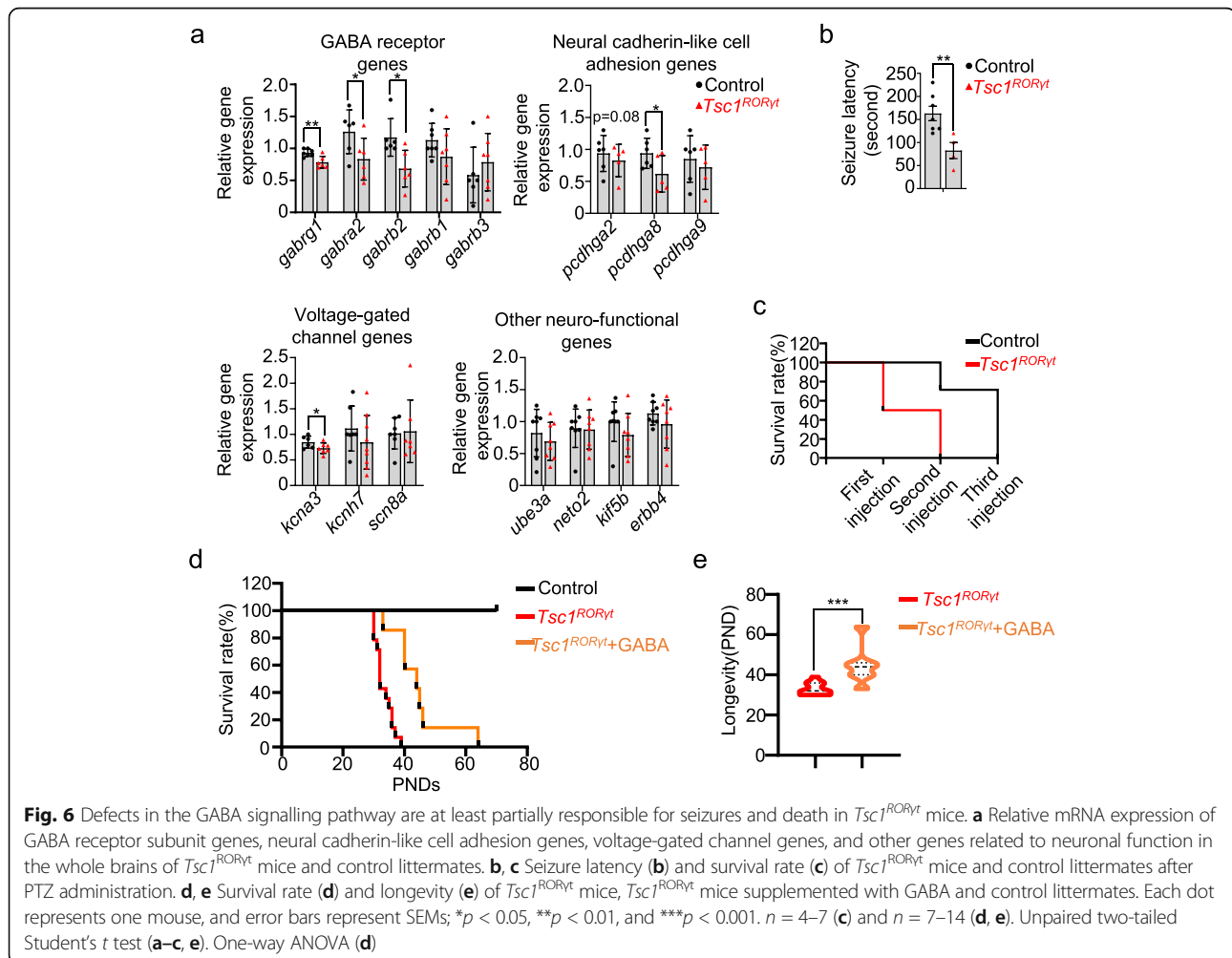
To further investigate the underlying mechanisms of these abnormalities in the nervous system, we measured

the gene expression levels of GABA receptor subunit genes (*gabrg1*, *gabra2*, *gabrb2*, *gabrb1*, and *gabrb3*), neural cadherin-like cell adhesion genes (*pcdhga2*, *pcdhga8*, and *pcdhga9*), voltage-gated channel subunits (*kcnh7*, *kcna3*, and *scn8a*), and other genes related to neuronal function (*ube3a*, *neto2*, *kif5b*, and *erbb4*) [36, 37] in the whole brains of both *Tsc1^{RORyt}* and control littermate mice by quantitative real-time RT-PCR. The GABA signaling pathway is the major inhibitory neural pathway and mediates slow and prolonged inhibitory activity [36], and defects in the GABA signaling pathway increase seizure susceptibility [38]. *Pcdhg* genes regulate neuronal survival, cortical interneuron programmed cell death, and neural circuit assembly [39, 40]. Sodium and potassium voltage-gated channel genes are also associated with neurological disorders [41–43]. Additionally, other genes have been reported to regulate neuronal function [44–47]. Notably, the expression levels of *gabrg1*, *gabra2*, and *gabrb2* were significantly downregulated in the brains of *Tsc1^{RORyt}* mice compared with control littermates. Additionally, *pcdhga2* and *pcdhga8*

and *kcna3* levels were decreased in the brains of *Tsc1^{RORyt}* mice (Fig. 6a).

To determine whether defects in the GABA signaling pathway resulted in seizures and death in the *Tsc1^{RORyt}* mice, the mice were injected with increasing doses of PTZ (a GABA receptor antagonist, 50 mg/kg, *i.p.*) [25], and the subsequent latency of generalized tonic-clonic seizures was determined. Compared with control littermates, *Tsc1^{RORyt}* mice showed a significant reduction in seizure latency (162.8 ± 41.5 s vs. 82.5 ± 35.0 s, respectively) after PTZ challenge (Fig. 6b). In addition, *Tsc1^{RORyt}* mice exhibited a 50% mortality rate after the first PTZ injection and 100% mortality rate after a second PTZ injection, while control littermates began to die with a 30% mortality rate after the second PTZ injection, and all died after the third PTZ injection (Fig. 6c).

To confirm the role of deficiency in the GABA signaling pathway in the death of *Tsc1^{RORyt}* mice, the mice were fed GABA through the drinking water starting at the age of 3 weeks after weaning. Although GABA supplementation did not prevent the death of the *Tsc1^{RORyt}*



mice, their survival time was prolonged, with a median value of 44 days (Fig. 6d, e). These data reveal that *Tsc1* deficiency in RORyt-expressing cells led to defects in the GABA signaling pathway that at least partially contributed to seizures and death in *Tsc1*^{RORyt} mice.

Presence of a group of rare RORyt-positive cells with a high metabolic level in the mouse brain

The deletion of *Tsc1* in RORyt-expressing cells did not affect ILC3s or Th17 cells; therefore, we speculated that a group of RORyt-expressing cells may be present in the brain and that the deletion of *Tsc1* in these cells would induce brain dysfunction, resulting in seizures, and eventual death. Therefore, we first analyzed RORyt expression in the whole brain by using data from the Allen Brain Atlas (<http://mouse.brain-map.org/>). Indeed, in situ hybridization (ISH) analysis indicated that RORyt was expressed in the cortex of the cerebrum and cerebellum during the embryonic period (E18.5). After birth, its expression increased and peaked at PNDs 14 and then decreased at PNDs 28 (Supplemental Fig. 2). Moreover, our RT-PCR and Western blotting data showed a very low level of RORyt expression in the brain that is much lower than its expression in the thymus (Fig. 7a, b). Therefore, we confirmed that, although rare, RORyt-positive cells are present in the brain.

By re-analyzing published single-cell RNA-seq data from the mouse brain [26], we identified 81 RORyt-positive cells among 11,069 cells (0.73% of total cells) (Fig. 7c). Functional enrichment analysis revealed that these RORyt-positive cells exhibited high expression levels of ribosomal and spliceosome-associated genes. Many of the highly expressed genes in RORyt-positive cells are also involved in both oxidative phosphorylation and neurological disorders, including Parkinson's disease, Huntington's disease, and Alzheimer's disease (Fig. 7d). Meanwhile, KEGG enrichment analysis indicated that 139 signaling pathways were significantly differently enriched between RORyt-positive cells and RORyt-negative cells (Supplemental Table 3). Among these pathways, many pathways related to metabolism, including glycosphingolipid biosynthesis and amino acid and fatty acid metabolism, were enriched in RORyt-positive cells, indicating that the metabolic level in RORyt-positive cells is enhanced compared to that of RORyt-negative cells in the brain (Fig. 7e). These data suggest the presence of a group of rare RORyt-positive cells with a high metabolic level in the mouse brain.

Discussion

Our study shows that *Tsc1* expression in RORyt-expressing cells is dispensable for ILC3 development and function but critical for brain homeostasis. Loss of *Tsc1* in RORyt-expressing cells in the mouse brain induced

neuronal defects, astrogliosis in the cortex and hippocampus, spontaneous tonic-clonic seizures, and death. Notably, GABA supplementation delayed death and prolonged lifespan to some extent.

According to previous studies, Th17 cells can infiltrate the brains of patients of Parkinson's disease and induce neuronal cell death [48], and *Tsc1* deficiency affects T cell development and function [9, 10]. However, our data showed that knockout of *Tsc1* in RORyt-expressing cells did not affect the development of Th17 cells; however, *Tsc1* knockout caused severe brain damage followed by death at the age of 4 to 6 weeks. Previous studies reported that neuron-specific inactivation of *Tsc1* resulted in the increased generation of neural progeny and death with a median survival time of 18 days [7], while the specific inactivation of *Tsc1* in GFAP-positive astrocytes led to astrogliosis and death between 11 and 22 weeks after birth [8]. These mice with astrocyte- and neuron-specific inactivation of *Tsc1* had an enlarged brain and edema. However, the brains of our model *Tsc1*^{RORyt} mice showed a normal appearance. The loss of *Tsc1* in RORyt-expressing cells not only caused neuronal defects but also induced astrogliosis, indicating that epilepsy and death caused by the inactivation of *Tsc1* in RORyt-expressing cells might be due to both the abnormal discharge of neurons and activated astrocytes. Because RORyt is expressed in the brain during the embryonic period (E18.5), the *Tsc1* gene was knocked out in RORyt-expressing cells in utero. Based on the findings, abnormal brain structures might appear during embryonic development, and a vicious circle between a disordered brain structure and seizures further aggravates brain damage with increasing age.

GABA, the major neurotransmitter in the central nervous system, is an important regulator of neuronal inhibition as it binds GABA_A receptors, which are ligand-gated anion channels. Dysfunction or mutation of GABA_A receptors has been identified in patients with various types of epilepsy [49]. *Tsc1*^{RORyt} mice exhibited a decreased latency to PTZ-induced seizures and were more susceptible to PTZ than control littermates, potentially due to decreased expression of GABA_A receptor subunits in the brain. Moreover, GABA supplementation prolonged the lifespan of *Tsc1*^{RORyt} mice, which further suggests that the impairment of GABA-GABA_A receptor interactions exacerbated seizures. Meanwhile, the loss of *Tsc1* in RORyt-expressing cells also decreased the expression levels of neuronal function-related genes (*pcdhga2* and *pcdhga8*) and ion channel gene expression (*kcnk3*). *Pcdhg* genes were reported to regulate neuronal survival, synaptic maintenance, and neural circuit assembly [40, 50], which might explain why GABA supplementation alone did not improve the survival rate of *Tsc1*^{RORyt} mice. The *Kcnk3* gene encodes the voltage-

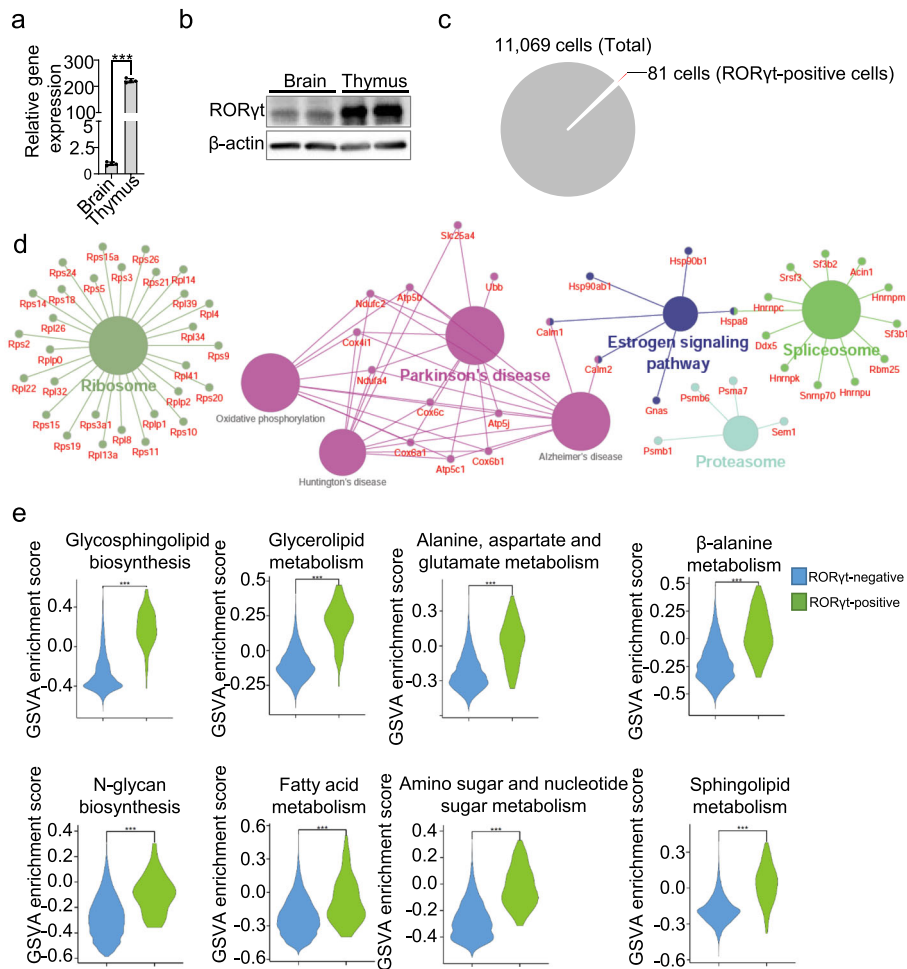


Fig. 7 A group of rare RORγt-positive cells with a high metabolic level exists in the mouse brain. **a, b** Relative expression of the RORγt mRNA in the whole brain and thymus (**a**) and RORγt protein expression in the whole brains (**b**) of mice at PNDs 14. **c** Proportion of RORγt-positive cells among total brain cells. **d** Functional enrichment analysis of the top 25% most highly expressed genes in RORγt-positive cells. **e** Functional gene sets identified by KEGG pathway enrichment analysis indicated increased metabolic pathway enrichment in RORγt-positive cells compared with RORγt-negative cells. Each dot represents one mouse, and error bars represent SEMs; ****p* < 0.001. Unpaired two-tailed Student's *t* test (**a**). Wilcoxon test (**e**)

gated potassium channel Kv1.3, which protects against neuro-inflammation [43, 51–53]. Thus, we proposed that the decreased expression of *kcnk3* was a compensatory mechanism when neuronal defects and astrogliosis occurred in the brains of *Tsc1*^{RORγt} mice.

According to the Allen Brain Atlas, RORγt is expressed in the brain during the embryonic period, and its expression increases after birth. In our study, the expression of RORγt in the brain parenchyma was confirmed by RT-PCR and Western blot analysis and then verified by analysis of published single-cell RNA-seq data. Interestingly, these rare RORγt-positive cells were found to be critical for brain homeostasis. Compared with RORγt-negative cells, RORγt-positive cells exhibited an increased metabolic level, as evidenced by higher levels of ribosomal gene expression and oxidative

phosphorylation. Oxidative phosphorylation is an essential process for cell function, and ribosomes are targeted for autophagy-mediated degradation to provide supplemental amino acids and nucleotides under conditions of nutrient starvation [54].

A recent study identified a cluster of RORγt-positive γδ T cells in the meninges that regulates anxiety-like behavior via IL-17a signaling in neurons [55]. These meningeal γδ T cells are virtually absent from the prenatal dural meninges but undergo progressive seeding after birth. However, we found that RORγt is expressed in the brain parenchyma during the embryonic period. In other words, the RORγt-positive cells in the brain parenchyma identified in the present study might not originate from the meninges. However, we were unable to exclude the possibility that *Tsc1* deletion in these meningeal γδ17 T

cells would also contribute to brain damage and death, as meningeal $\gamma\delta 17$ T cells also express RORyt at high levels. A limitation of the study is that we did not determine the location, type or source of these RORyt-positive cells.

Conclusions

Taken together, our results verify the critical role of previously unnoticed RORyt-expressing cells in the brain and indicate that the Tsc1 signaling pathway in RORyt-expressing cells is important for maintaining neuron and astrocyte homeostasis.

Abbreviations

Tsc1: Tuberous sclerosis complex 1; Tsc2: Tuberous sclerosis complex 2; ILCs: Innate lymphoid cells; LTi cells: Lymphoid tissue inducer cells; PND: Postnatal day; LPL: Lamina propria layer; HE: Hematoxylin-eosin; ECG: Electrocardiogram; NeuN: Neuronal nuclei antigen; DG: Dentate gyrus; GFAP: Glial fibrillary acidic protein; GABA: γ -Amino butyric acid; PTZ: Pentylentetrazole; ISH: In situ hybridization

Supplementary Information

The online version contains supplementary material available at <https://doi.org/10.1186/s12974-021-02153-8>.

Additional file 1: Supplemental Fig. 1. Abnormal activation of neurons and astrogliosis in the cortex and hippocampus of $Tsc1^{RORyt}$ mice. a and b Representative images of Nissl staining (a) and GFAP immunostaining (green) (b) in the brains of $Tsc1^{RORyt}$ mice and control littermates. All images were captured from scans of whole-brain slices. Magnification: 5x (a and b). Scale bars: 200 μ m (a and b).

Additional file 2: Supplemental Fig. 2. RORyt expression in the mouse brain at different periods. ISH analysis revealed RORyt expression during the embryonic period (E18.5) and at PNDs 4, PNDs 14 and PNDs 28. All ISH data were obtained from Allen Brain Map: Developing Mouse Brain Atlas (<http://developingmouse.brain-map.org>). Image credit: Allen Institute.

Additional file 3: Supplemental Table 1. Antibodies used for flow cytometry and immunofluorescence staining.

Additional file 4: Supplemental Table 2. Primer pairs used for RT-PCR.

Additional file 5: Supplemental Table 3. KEGG analysis of different signal pathway between RORyt-positive cells and RORyt-negative cells.

Additional file 6: Supplemental Video 1. Video showing a two-week-old $Tsc1^{RORyt}$ mouse experiencing spontaneous seizures.

Additional file 7: Supplemental Video 2. Video showing a four-week-old $Tsc1^{RORyt}$ mouse experiencing spontaneous seizures, ultimately resulting in wild jumping and death.

Acknowledgements

The authors would like to thank Professors Peng Li, Fengchao Wang, and Jiada Li for professional analyses of HE staining results from mouse tissues and organs.

Authors' contributions

Y.F.D., L.L., Y.D. and X.L. designed the project and analyzed the data. Y.F.D., Y.D., and X.L. wrote the manuscript. Q.Y., Y.Y., Y.L., and H.P. performed the animal experiments. Q.Y., S.W., and B.Y. performed the RT-PCR assays and Western blot analyses. S.L. and Y.G. provided experimental suggestions or provided experimental materials for this study. All authors read and approved the final manuscript.

Funding

This study was supported by grants from the National Natural Science Foundation of China (No. 81773742 to X.L.; No. 81703521 to Y.F.D.; and Nos.

81874313 and 81922068 to Y.C.D.) and the Natural Science Foundation of Hunan Province (No. 2020JJ5279 to Y.F.D.).

Availability of data and materials

The authors declare that all data in support of the findings of this study are available within the article and its supplementary information files or from the corresponding author (Dr. Youcai Deng, youcai.deng@tmmu.edu.cn) upon reasonable request.

Declarations

Ethics approval and consent to participate

All animal protocols and experiments were performed according to the Guide for the Care and Use of Laboratory Animals and the guidelines of the Institutional Animal Care and Use Committee of Hunan Children's Hospital and were approved by the Animal Ethics Committee of Hunan Children's Hospital.

Consent for publication

Not applicable.

Competing interests

The authors declare that they have no competing interests.

Author details

¹Hunan Children's Research Institute (HCRI), Hunan Children's Hospital, Changsha 410000, China. ²Institute of Materia Medica, College of Pharmacy, Army Medical University (Third Military Medical University), Chongqing 400038, China. ³Department of Pharmacy, The Third Xiangya Hospital, Central South University, Changsha 410000, China. ⁴Department of Clinical Biochemistry, Faculty of Pharmacy and Laboratory Medicine, Army Medical University (Third Military Medical University), Chongqing 400038, China. ⁵Southwest Hospital/Southwest Eye Hospital, Third Military Medical University, Chongqing 400038, China.

Received: 15 January 2021 Accepted: 15 April 2021

Published online: 06 May 2021

References

- Kim J, Guan KL. mTOR as a central hub of nutrient signalling and cell growth. *Nat Cell Biol.* 2019;21(1):63–71. <https://doi.org/10.1038/s41556-018-0205-1>.
- Inoki K, Corradetti MN, Guan KL. Dysregulation of the TSC-mTOR pathway in human disease. *Nat Genet.* 2005;37(1):19–24. <https://doi.org/10.1038/ng1494>.
- Zoncu R, Efeyan A, Sabatini DM. mTOR: from growth signal integration to cancer, diabetes and ageing. *Nat Rev Mol Cell Biol.* 2011;12(1):21–35. <https://doi.org/10.1038/nrm3025>.
- Kobayashi T, Minowa O, Sugitani Y, Takai S, Mitani H, Kobayashi E, et al. A germ-line Tsc1 mutation causes tumor development and embryonic lethality that are similar, but not identical to, those caused by Tsc2 mutation in mice. *Proc Natl Acad Sci U S A.* 2001;98(15):8762–7. <https://doi.org/10.1073/pnas.151033798>.
- Crino PB. The mTOR signalling cascade: paving new roads to cure neurological disease. *Nat Rev Neurol.* 2016;12(7):379–92. <https://doi.org/10.1038/nrneuro.2016.81>.
- Zhou J, Shrikhande G, Xu J, McKay RM, Burns DK, Johnson JE, et al. Tsc1 mutant neural stem/progenitor cells exhibit migration deficits and give rise to subependymal lesions in the lateral ventricle. *Genes Dev.* 2011;25(15):1595–600. <https://doi.org/10.1101/gad.16750211>.
- Magri L, Cambiaghi M, Cominelli M, Alfaro-Cervello C, Cursi M, Pala M, et al. Sustained activation of mTOR pathway in embryonic neural stem cells leads to development of tuberous sclerosis complex-associated lesions. *Cell Stem Cell.* 2011;9(5):447–62. <https://doi.org/10.1016/j.stem.2011.09.008>.
- Uhlmann EJ, Wong M, Baldwin RL, Bajenaru ML, Onda H, Kwiatkowski DJ, et al. Astrocyte-specific TSC1 conditional knockout mice exhibit abnormal neuronal organization and seizures. *Ann Neurol.* 2002;52(3):285–96. <https://doi.org/10.1002/ana.10283>.
- Yang K, Neale G, Green DR, He W, Chi H. The tumor suppressor Tsc1 enforces quiescence of naive T cells to promote immune homeostasis and function. *Nat Immunol.* 2011;12(9):888–97. <https://doi.org/10.1038/ni.2068>.

10. Park Y, Jin HS, Lopez J, Elly C, Kim G, Murai M, et al. TSC1 regulates the balance between effector and regulatory T cells. *J Clin Invest*. 2013;123(12):5165–78. <https://doi.org/10.1172/JCI69751>.
11. Yang M, Chen S, Du J, He J, Wang Y, Li Z, et al. NK cell development requires Tsc1-dependent negative regulation of IL-15-triggered mTORC1 activation. *Nat Commun*. 2016;7(1):12730. <https://doi.org/10.1038/ncomms12730>.
12. Bogunovic M. ILC3s and the willow tree of voices. *Immunity*. 2016;45(2):238–9. <https://doi.org/10.1016/j.immuni.2016.08.004>.
13. Korn T, Bettelli E, Oukka M, Kuchroo VK. IL-17 and Th17 Cells. *Annu Rev Immunol*. 2009;27(1):485–517. <https://doi.org/10.1146/annurev.immunol.021908.132710>.
14. Eberl G, Marmon S, Sunshine MJ, Rennert PD, Choi Y, Littman DR. An essential function for the nuclear receptor ROR γ (t) in the generation of fetal lymphoid tissue inducer cells. *Nat Immunol*. 2004;5(1):64–73. <https://doi.org/10.1038/ni1022>.
15. Sanos SL, Bui VL, Mortha A, Oberle K, Heners C, Johner C, et al. ROR γ t and commensal microflora are required for the differentiation of mucosal interleukin 22-producing NKp46(+) cells. *Nature Immunology*. 2009;10(1):83–91. <https://doi.org/10.1038/ni1684>.
16. Eberl G, Littman DR. Thymic origin of intestinal alphabeta T cells revealed by fate mapping of ROR γ mat+ cells. *Science*. 2004;305(5681):248–51. <https://doi.org/10.1126/science.1096472>.
17. Kwiatkowski DJ, Zhang H, Bandura JL, Heiberger KM, Glogauer M, el-Hashemite N, et al. A mouse model of TSC1 reveals sex-dependent lethality from liver hemangiomas, and up-regulation of p70S6 kinase activity in Tsc1 null cells. *Hum Mol Genet*. 2002;11(5):525–34. <https://doi.org/10.1093/hmg/11.5.525>.
18. Deng Y, Wu S, Yang Y, Meng M, Chen X, Chen S, et al. Unique Phenotypes of Heart Resident Type 2 Innate Lymphoid Cells. *Front Immunol*. 2020;11:802. <https://doi.org/10.3389/fimmu.2020.00802>.
19. Wang F, Meng M, Mo B, Yang Y, Ji Y, Huang P, et al. Crosstalks between mTORC1 and mTORC2 variate cytokine signaling to control NK maturation and effector function. *Nat Commun*. 2018;9(1):4874. <https://doi.org/10.1038/s41467-018-07277-9>.
20. Huang P, Wang F, Yang Y, Lai W, Meng M, Wu S, et al. Hematopoietic-Specific Deletion of Foxo1 Promotes NK Cell Specification and Proliferation. *Front Immunol*. 2019;10:1016. <https://doi.org/10.3389/fimmu.2019.01016>.
21. Zhang Q, Deng Y, Lai W, Guan X, Sun X, Han Q, et al. Maternal inflammation activated ROS-p38 MAPK predisposes offspring to heart damages caused by isoproterenol via augmenting ROS generation. *Sci Rep*. 2016;6(1):30146. <https://doi.org/10.1038/srep30146>.
22. Korzhvskii DE, Otellin VA. Immunocytochemical detection of astrocytes in brain slices in combination with Nissl staining. *Neurosci Behav Physiol*. 2005;35(6):639–41. <https://doi.org/10.1007/s11055-005-0105-2>.
23. Deng Y, Zhang Q, Luo H, Chen X, Han Q, Wang F, et al. Sustained elevation of NF- κ B activity sensitizes offspring of maternal inflammation to hypertension via impairing PGC-1 α recovery. *Sci Rep*. 2016;6(1):32642. <https://doi.org/10.1038/srep32642>.
24. Deng Y, Kerdiles Y, Chu J, Yuan S, Wang Y, Chen X, et al. Transcription factor Foxo1 is a negative regulator of natural killer cell maturation and function. *Immunity*. 2015;42(3):457–70. <https://doi.org/10.1016/j.immuni.2015.02.006>.
25. Feliciano DM, Su T, Lopez J, Platel JC, Bordey A. Single-cell Tsc1 knockout during corticogenesis generates tuber-like lesions and reduces seizure threshold in mice. *J Clin Invest*. 2011;121(4):1596–607. <https://doi.org/10.1172/JCI44909>.
26. Loo L, Simon JM, Xing L, McCoy ES, Niehaus JK, Guo J, et al. Single-cell transcriptomic analysis of mouse neocortical development. *Nat Commun*. 2019;10(1):134. <https://doi.org/10.1038/s41467-018-08079-9>.
27. Stuart T, Butler A, Hoffman P, Hafemeister C, Papalexi E, Mauck WM 3rd, et al. Comprehensive Integration of Single-Cell Data. *Cell*. 2019;177:1888–902 e1821.
28. Bindea G, Mlecnik B, Hackl H, Charoentong P, Tosolini M, Kirilovsky A, et al. ClueGO: a Cytoscape plug-in to decipher functionally grouped gene ontology and pathway annotation networks. *Bioinformatics*. 2009;25(8):1091–3. <https://doi.org/10.1093/bioinformatics/btp101>.
29. Hänzelmann S, Castelo R, Guinney J. GSEA: gene set variation analysis for microarray and RNA-seq data. *BMC Bioinformatics*. 2013;14(1):7. <https://doi.org/10.1186/1471-2105-14-7>.
30. Yang Y, Deng X, Chen X, Chen S, Song L, Meng M, et al. Landscape of active enhancers developed de novo in cirrhosis and conserved in hepatocellular carcinoma. *Am J Cancer Res*. 2020;10(10):3157–78.
31. Diefenbach A, Colonna M, Koyasu S. Development, differentiation, and diversity of innate lymphoid cells. *Immunity*. 2014;41(3):354–65. <https://doi.org/10.1016/j.immuni.2014.09.005>.
32. Amiri M, Bahrami F, Janahmadi M. Functional contributions of astrocytes in synchronization of a neuronal network model. *J Theor Biol*. 2012;292:60–70. <https://doi.org/10.1016/j.jtbi.2011.09.013>.
33. Zhao BB, Chen LL, Long QH, Xie GJ, Xu B, Li ZF, et al. Preventive effects of escitalopram against anxiety-like depressive behaviors in monosodium glutamate-treated rats subjected to partial hepatectomy. *Front Psychol*. 2019;10:2462. <https://doi.org/10.3389/fpsyg.2019.02462>.
34. Way SW, McKenna J 3rd, Mietzsch U, Reith RM, Wu HC, Gambello MJ. Loss of Tsc2 in radial glia models the brain pathology of tuberous sclerosis complex in the mouse. *Hum Mol Genet*. 2009;18(7):1252–65. <https://doi.org/10.1093/hmg/ddp025>.
35. Zhao X, Liao Y, Morgan S, Mathur R, Feustel P, Mazurkiewicz J, et al. Noninflammatory changes of microglia are sufficient to cause epilepsy. *Cell Rep*. 2018;22(8):2080–93. <https://doi.org/10.1016/j.celrep.2018.02.004>.
36. Watanabe M, Maemura K, Kanbara K, Tamayama T, Hayasaki H. GABA and GABA receptors in the central nervous system and other organs. *Int Rev Cytol*. 2002;213:1–47. [https://doi.org/10.1016/S0074-7696\(02\)13011-7](https://doi.org/10.1016/S0074-7696(02)13011-7).
37. Manford M. Recent advances in epilepsy. *J Neurol*. 2017;264(8):1811–24. <https://doi.org/10.1007/s00415-017-8394-2>.
38. Olson CA, Vuong HE, Yano JM, Liang QY, Nusbaum DJ, Hsiao EY. The gut microbiota mediates the anti-seizure effects of the ketogenic diet. *Cell*. 2018;173(7):1728–41 e1713. <https://doi.org/10.1016/j.cell.2018.04.027>.
39. Mancia Leon WR, Spatazza J, Rakela B, Chatterjee A, Pande V, Maniatis T, et al. Clustered gamma-protocadherins regulate cortical interneuron programmed cell death. *Elife*. 2020;9. <https://doi.org/10.7554/eLife.55374>.
40. Mountoufaris G, Chen WW, Hirabayashi Y, O'Keefe S, Chevee M, Nwazike CL, et al. Multicenter Pcdh diversity is required for mouse olfactory neural circuit assembly. *Science*. 2017;356(6336):411–4. <https://doi.org/10.1126/science.aai8801>.
41. Ohba C, Kato M, Takahashi S, Lerman-Sagie T, Lev D, Terashima H, et al. Early onset epileptic encephalopathy caused by de novo SCN8A mutations. *Epilepsia*. 2014;55(7):994–1000. <https://doi.org/10.1111/epi.12668>.
42. Li W, Yin L, Shen C, Hu K, Ge J, Sun A. SCN5A variants: association with cardiac disorders. *Front Physiol*. 2018;9:1372. <https://doi.org/10.3389/fphys.2018.01372>.
43. Fomina AF, Nguyen HM, Wulff H. Kv1.3 inhibition attenuates neuroinflammation through disruption of microglial calcium signaling. *Channels (Austin)*. 2021;15(1):67–78. <https://doi.org/10.1080/19336950.2020.1853943>.
44. Mahadevan V, Dargaei Z, Ivakine EA, Hartmann AM, Ng D, Chevrier J, et al. Neto2-null mice have impaired GABAergic inhibition and are susceptible to seizures. *Front Cell Neurosci*. 2015;9:368.
45. Nakajima K, Yin X, Takei Y, Seog DH, Homma N, Hirokawa N. Molecular motor KIF5A is essential for GABA(A) receptor transport, and KIF5A deletion causes epilepsy. *Neuron*. 2012;76(5):945–61. <https://doi.org/10.1016/j.neuron.2012.10.012>.
46. Deng W, Luo F, Li BM, Mei L. NRG1-ErbB4 signaling promotes functional recovery in a murine model of traumatic brain injury via regulation of GABA release. *Exp Brain Res*. 2019;237(12):3351–62. <https://doi.org/10.1007/s00221-019-05680-2>.
47. Berrios J, Stamatakis AM, Kantak PA, McElligott ZA, Judson MC, Aita M, et al. Loss of UBE3A from TH-expressing neurons suppresses GABA co-release and enhances VTA-NAC optical self-stimulation. *Nat Commun*. 2016;7(1):10702. <https://doi.org/10.1038/ncomms10702>.
48. Sommer A, Maxreiter F, Krach F, Fadler T, Grosch J, Maroni M, et al. Th17 Lymphocytes Induce Neuronal Cell Death in a Human iPSC-Based Model of Parkinson's Disease. *Cell Stem Cell*. 2018;23(1):123–31 e126. <https://doi.org/10.1016/j.stem.2018.06.015>.
49. Butler KM, Moody OA, Schuler E, Coryell J, Alexander JJ, Jenkins A, et al. De novo variants in GABRA2 and GABRA5 alter receptor function and contribute to early-onset epilepsy. *Brain*. 2018;141(8):2392–405. <https://doi.org/10.1093/brain/awy171>.
50. Ing-Esteves S, Kostadinov D, Marocha J, Sing AD, Joseph KS, Laboulaye MA, et al. Combinatorial effects of alpha- and gamma-protocadherins on

- neuronal survival and dendritic self-avoidance. *J Neurosci.* 2018;38(11):2713–29. <https://doi.org/10.1523/JNEUROSCI.3035-17.2018>.
51. Chen YJ, Nguyen HM, Maezawa I, Jin LW, Wulff H. Inhibition of the potassium channel Kv1.3 reduces infarction and inflammation in ischemic stroke. *Ann Clin Transl Neurol.* 2018;5(2):147–61. <https://doi.org/10.1002/actn3.513>.
 52. Ma DC, Zhang NN, Zhang YN, Chen HS. Kv1.3 channel blockade alleviates cerebral ischemia/reperfusion injury by reshaping M1/M2 phenotypes and compromising the activation of NLRP3 inflammasome in microglia. *Exp Neurol.* 2020;332:113399.
 53. Maezawa I, Nguyen HM, Di Lucente J, Jenkins DP, Singh V, Hilt S, et al. Kv1.3 inhibition as a potential microglia-targeted therapy for Alzheimer's disease: preclinical proof of concept. *Brain.* 2018;141:596–612.
 54. Wyant GA, Abu-Remaileh M, Frenkel EM, Laqtom NN, Dharamdasani V, Lewis CA, et al. NUFIP1 is a ribosome receptor for starvation-induced ribophagy. *Science.* 2018;360(6390):751–8. <https://doi.org/10.1126/science.aar2663>.
 55. Alves de Lima K, Rustenhoven J, Da Mesquita S, Wall M, Salvador AF, Smirnov I, et al. Meningeal $\gamma\delta$ T cells regulate anxiety-like behavior via IL-17a signaling in neurons. *Nat Immunol.* 2020;21(11):1421–9. <https://doi.org/10.1038/s41590-020-0776-4>.

Publisher's Note

Springer Nature remains neutral with regard to jurisdictional claims in published maps and institutional affiliations.

Ready to submit your research? Choose BMC and benefit from:

- fast, convenient online submission
- thorough peer review by experienced researchers in your field
- rapid publication on acceptance
- support for research data, including large and complex data types
- gold Open Access which fosters wider collaboration and increased citations
- maximum visibility for your research: over 100M website views per year

At BMC, research is always in progress.

Learn more biomedcentral.com/submissions

